ROYAL SOCIETY
OF CHEMISTRY

PAPER

Water activity and electrocrystallization modulated by a high-Lewis-basicity co-solvent for reversible Zn anodes†

Qiang Zhang, Hefei Fan, Jianxin Gao and Erdong Wang (ID) *

Aqueous rechargeable zinc metal batteries exhibit significant potential for large-scale energy storage due to their environmental friendliness, high safety and low cost. However, the severe hydrogen evolution reaction, uncontrollable dendrite growth and low coulombic efficiency of the Zn metal anode hinders their further application. Herein, high-basicity N-methylacetamide (NMA), which can anchor water molecules *via* strong hydrogen bonds, is introduced as a co-solvent into a 1 M $ZnSO_4$ electrolyte, thus reducing the decomposition activity of water molecules. Additionally, the NMA molecules and SO_4^{2-} interact with the Zn^{2+} solvation sheath to release water molecules around Zn^{2+} and further reduce the HER. Moreover, the NMA-based electrolyte promotes Zn (002) deposition, improving the intrinsic corrosion resistance and uniform deposition of the zinc anode. At 1 mA cm^{-2}, the Zn//Cu battery achieves a high average coulombic efficiency of 99.85% for 1200 cycles. The Zn//Zn symmetric battery delivers a long lifespan of more than 900 h even at high areal capacity (6 mA h cm^{-2}) and high depth of discharge (DOD ≈ 50%) conditions. The Zn//NaV$_3$O$_8$ full battery undergoes 300 cycles with a capacity retention of 82.7% at 0.1 A g^{-1} under a low negative/positive capacity (N/P) ratio of 3.24 and high discharge depth of the zinc metal anode (DOD ≈ 30.8%).

Broader context

Aqueous rechargeable zinc metal batteries exhibit significant potential for large-scale energy storage due to their environmental friendliness, high safety and low cost. However, the severe hydrogen evolution reaction, uncontrollable dendrite growth and low coulombic efficiency of the Zn metal anode hinder their further application. Researchers have often focused on solvated water, *e.g.*, introducing high-donor-number solvents to release water molecules in the solvation sheath of Zn^{2+}, to reduce the hydrogen evolution reaction. In contrast, there is little research on free water molecules. Herein, high-basicity N-methylacetamide (NMA), which can anchor water molecules through strong hydrogen bonds, is introduced as a co-solvent into a 1 M $ZnSO_4$ electrolyte, thus reducing the decomposition activity of water molecules. Additionally, the NMA molecules and SO_4^{2-} interact with the Zn^{2+} solvation sheath to release water molecules around Zn^{2+} and further reduce the HER. Moreover, the NMA-based electrolyte promotes Zn (002) deposition, improving the intrinsic corrosion resistance and uniform deposition of the zinc anode. Undoubtedly, this work will further the practical application of zinc metal anodes in ZIBs.

1. Introduction

Rechargeable aqueous zinc metal batteries have undergone booming development in the field of electric grid energy storage with inherent environmentally friendly, nonflammable, and affordable features.[1-4] Zn metal exhibits outstanding electrochemical properties (high theoretical capacity of 820 mA h g^{-1} and 5855 mA h cm^{-3}, and relatively low electrochemical potential of −0.76 V *vs.* the standard hydrogen electrode (SHE)), high compatibility/stability, and has abundant natural reserves.[5-7] However, the widespread application of these batteries has encountered bottlenecks, especially the evolution of hydrogen, the generation of zinc dendrites, and by-product formation during cycling of the zinc anode.[8-10]

It was found that anodic zinc exhibited a more stable plating/stripping process when a deep eutectic solvent, a eutec-

Division of Fuel Cell & Battery, Dalian National Laboratory for Clean Energy, Dalian Institute of Chemical Physics, Chinese Academy of Sciences, Dalian 116023, China. E-mail: edwang@dicp.ac.cn

tic mixture of a Lewis/Brønsted acidic anion and an alkaline cation, was used as the electrolyte for zinc-based batteries.[11,12] Zhou[13] *et al.* proposed the use of a eutectic solution based on *N*-methylacetamide (NMA) instead of an aqueous solution as the electrolyte for the zinc–iodine battery. Chen[14] *et al.* designed dual-metal-salt-derived ternary eutectic electrolytes for ZIBs, which were constructed from zinc trifluoromethanesulfonate ($Zn(OTF)_2$), the supporting salt of lithium bis(trifluoromethanesulfonyl)imide, and the neutral ligand of *N*-methylacetamide (NMA). However, the disadvantage of poor Zn^{2+} diffusion efficiency caused by low electron conductivity and high viscosity was also prominent. Researchers have explored a variety of organic solvents (alcohols, ethers, sulfones, ketones, esters, *etc.*) as co-solvents in aqueous electrolytes to simultaneously change the solvation structure of Zn^{2+} and form hydrogen bonds with water molecules, thereby improving the electrochemical performance of the zinc metal anode.[15–19] These studies often focus on solvated water, *e.g.*, introducing high-donor-number solvents to release water molecules in the solvation sheath of Zn^{2+}, to reduce the hydrogen evolution reaction. In contrast, there is little research on free water molecules.[20] In aqueous electrolytes, the proportion of free water (about 90% in a 2 M $ZnSO_4$ solution) is much higher than that of solvated water. At the electrode/electrolyte interphase, the free water reacts readily with Zn metal, which plays a vital role in the hydrogen evolution reaction.[21] Accordingly, modifying the state of the free water molecules, thereby reducing their reactivity, represents an effective strategy for enhancing the reversibility of zinc metal anodes.[22–24]

Currently, the formation of hydrogen bonds between polar solvents and water molecules is the limited conventional method to inhibit free water activity.[25,26] Nevertheless, little attention has been paid to the type of solvent introduced and the strength of the hydrogen bonds formed. The decomposition activity of water can be effectively inhibited by the generation of stronger hydrogen bonds involving water *via* the adoption of a suitable solvent.[27,28] Naturally, the chosen solvent needs to have the characteristics of ultra-high hydrogen bond donor strength and a high dielectric constant (ε) to form strong hydrogen bonds and increase ionic conductivity.[29] Generally, the Kamlet–Taft (K–T) parameters of acidity or hydrogen bond donor strength (α), basicity or hydrogen bond acceptor strength (β) and polarizability ($\pi^\star$) can be used as a basis.[30] Based on this, solvents with low α values and high β and $\pi^\star$ values would be considered as suitable targets.

Herein, *N*-methylacetamide (NMA), which has a high hydrogen bond acceptor strength ($\beta = 0.80$), was introduced into a $ZnSO_4$ electrolyte as a co-solvent to prepare a mixed electrolyte. The decomposition activity of water molecules is significantly reduced due to the strong hydrogen bonds formed between the C=O of NMA and the H atoms of water molecules. Additionally, NMA molecules promote the entry of small amounts of SO_4^{2-} into the solvation sheath of Zn^{2+}, thus releasing water molecules around Zn^{2+} and further reducing the hydrogen evolution performance. Moreover, the NMA-based electrolyte induces the preferential deposition of the Zn

(002) crystal plane, which improves the intrinsic corrosion resistance and uniform deposition ability of the zinc anode, promoting higher reversibility of the zinc deposition/dissolution reaction and achieving flatter and denser zinc deposition. At a low current density of 1 mA cm^{-2}, the average coulombic efficiency of the zinc metal anode during 1200 cycles is as high as 99.85%, which is much higher than the performance in 1 M $ZnSO_4$ electrolyte (99.33%, 132 cycles). The Zn//Zn symmetric cell can work stably for 900 h at a high areal capacity 6 mA h cm^{-2} and discharge depth of DOD $\approx$ 50%. Encouragingly, even under a low capacity ratio of about 3.24 of Zn metal anode (DOD = 0.308) to the cathode ($\sim$3.7 mA h, 23.1 mg cm^{-2}), the Zn//NaV$_3$O$_8$ full cells also show better cycling stability in the NMA-based electrolyte (300 cycles) than in pure aqueous 1 M $ZnSO_4$ electrolyte (only 57 cycles).

2. Results and discussion

2.1 Structure analysis of the electrolyte

By introducing a suitable solvent, water can form strong hydrogen bonds, thereby inhibiting the decomposition activity of water. Based on this, the optimal solvent *N*-methylacetamide (NMA) with an ultra-high dielectric constant ($\varepsilon = 178.9$), high hydrogen bond acceptor strength ($\beta = 0.80$), high polarizability ($\pi^\star = 1.10$) and lower toxicity hazard (Table S1†) was introduced to $ZnSO_4$ electrolyte as a co-solvent to prepare a mixed electrolyte.[31] As shown in the digital photo of 1 M $ZnSO_4$ electrolytes with different NMA content (Fig. S1a†), when the NMA volume fraction reaches 40%, $ZnSO_4$ begins to precipitate from the solution. The physical and electrochemical properties of electrolytes with an NMA content below 35% were characterized. Due to the high viscosity of NMA (3.23 mPa s, 35 °C) and the promotion of the formation of contact ion pairs in the solution, the ionic conductivity of the electrolyte gradually decreases with increasing NMA volume fraction (Fig. S1b and c†), but it is still higher than that of the high-concentration electrolyte.[32] Additionally, the zinc ion transfer number of ZS-25%NMA and ZS electrolytes reach 0.79 and 0.66 (Fig. S2†), respectively.

Raman spectroscopy (Raman), Fourier transform infrared spectroscopy (FTIR) and nuclear magnetic resonance spectroscopy (NMR) were used to analyze the changes in the local structure of the electrolyte with increasing NMA content. The stretching vibration peak of SO_4^{2-} in the Raman spectrum (Fig. 1a) shows a gradual blue-shift as NMA is added to the $ZnSO_4$ electrolyte, indicating that NMA promotes the formation of contact ion pairs.[33] In fact, the NMA molecule has a weaker ability to dissolve $ZnSO_4$ (Fig. S1a†), despite its having a higher dielectric constant than the water molecule. As in previous research, SO_4^{2-} has a high negative charge density and exhibits a salting-out effect.[1] However, there are two hydrophobic methyl groups at both ends of the NMA molecule, which are incompatible with SO_4^{2-}. With the gradual increase of the NMA content, the interaction between SO_4^{2-} and Zn^{2+} is enhanced, eventually leading to the precipitation of $ZnSO_4$.[34]
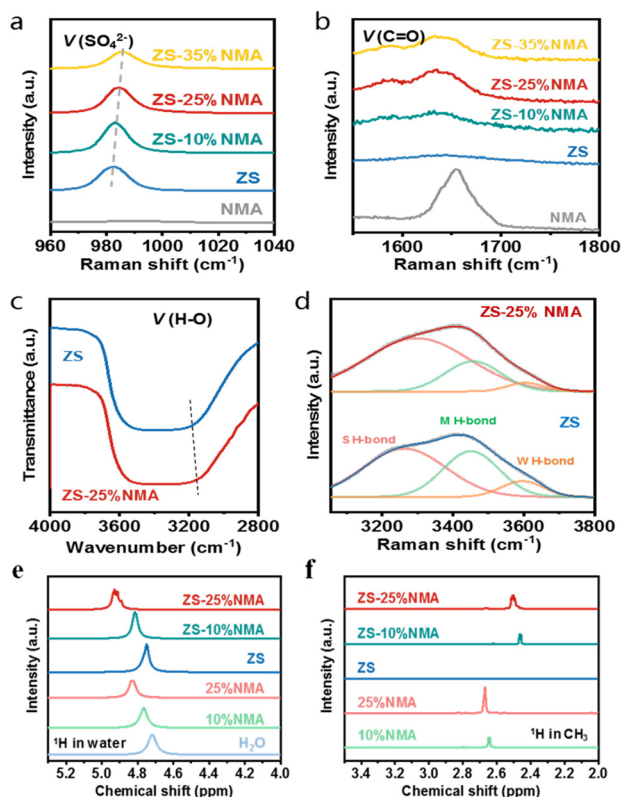
Fig. 1 Raman spectra of the different solutions: (a) stretching vibration of SO_4^{2-}; (b) stretching vibration of C=O. (c) FTIR spectra of different solutions. (d) Fitted Raman spectra of O–H stretching in different electrolytes. ^{1}H NMR spectrum of (e) water molecules and (f) –CH₃ (NMA) in different solutions.

Therefore, the activity of the water molecules can be reduced by promoting the formation of direct interaction between Zn^{2+} and SO_4^{2-} *via* introducing an appropriate amount of NMA molecules, due to some water molecules around Zn^{2+} being expelled. In the Raman spectrum (Fig. 1b), upon mixing with water molecules, the C=O stretching vibration peak of NMA at 1654 cm^{-1} moves to lower wavenumber, proving the generation of hydrogen bond interactions between water molecules and NMA molecules.[35] The FTIR spectrum (Fig. 1c) also demonstrates that the O–H stretching vibration peak exhibits an obvious red-shift with the introduction of NMA molecules, once again verifying that NMA changes the original hydrogen bond network of the water molecules.[36] The hydrogen bond peaks at 3050–3800 cm^{-1} can be divided into three characteristic peaks, corresponding to strong hydrogen bonds, medium-strength hydrogen bonds and weak hydrogen bonds.[37] After the incorporation of NMA, there is a notable increase in strong hydrogen bonds at the low wavenumber range (Fig. 1d). Concurrently, a marked diminution of weak hydrogen bonds is observed at high wavenumber. This phenomenon underscores the capacity of NMA molecules to firmly anchor water molecules *via* strong hydrogen bond interactions, consequently mitigating their propensity for decomposition. Density functional theory (DFT) was used to calculate the interaction

between NMA and H_2O. As shown in Fig. S3,† the binding energy between NMA and H_2O is significantly higher than that between H_2O molecules, and in particular, the NMA (C=O)–H_2O interaction is stronger. Therefore, NMA mainly forms strong hydrogen bonds with H_2O through C=O, thereby effectively inhibiting the hydrogen evolution reaction on the surface of the zinc metal anode.[32,38,39]

Fig. 1e and f show the ^{1}H nuclear magnetic resonance (NMR) spectra of different electrolytes. The addition of zinc sulphate to water shifts the ^{1}H chemical shift of water molecules to lower field (increased δ) (Fig. 1e), indicating that the electron cloud density around the H atoms decreases, which is caused by the coordination of the water molecules with Zn^{2+}. Additionally, the ^{1}H chemical shift exhibits a congruent directional trend upon the introduction of *N*-methylacetamide (NMA) molecules to water, thereby corroborating the presence of hydrogen bonding interactions between NMA molecules and water molecules. Moreover, the magnitude of the chemical shift increment is correlated with the concentration of NMA molecules, suggesting a progressive enhancement in the hydrogen bond interaction. When NMA is added to the aqueous zinc sulfate electrolyte, the chemical shift still shows an increasing trend. Thus, NMA molecules may have two interactions in the electrolyte, forming hydrogen bonds with water molecules and participating in the formation of the Zn^{2+} solvation sheath. If an NMA molecule has a direct interaction with Zn^{2+}, some water molecules around Zn^{2+} will be released, thereby causing the ^{1}H chemical shift of the water molecules to move to higher field. Therefore, in the aqueous ZS-NMA electrolyte, the main role of the NMA molecules is to generate hydrogen bonds with water molecules. In addition, the ^{1}H NMR spectra of the methyl group was used to further analyze whether an interaction between the NMA molecule and Zn^{2+} existed. Obviously, when zinc sulfate was added to the NMA–H_2O mixed solution, the ^{1}H chemical shift moved to higher field (Fig. 1f), confirming the entry of NMA molecules into the Zn^{2+} solvation sheath.[37,40]

To reveal the local structure of the electrolyte in detail, molecular dynamics simulation (MD) was used to study the interactions among Zn^{2+}, SO_4^{2-}, H_2O and NMA. The corresponding radial distribution function (RDF) and coordination number (CN) distribution function in different environments (H_2O, NMA and SO_4^{2-}) around Zn^{2+} in the electrolyte and the environment around the NMA molecules were obtained through MD simulation. As shown in Fig. 2a and b, in 1 M $ZnSO_4$ electrolyte, the Zn^{2+}–H_2O and Zn^{2+}–SO_4^{2-} peaks appear at about 2.15 Å and 2.55 Å, with coordination numbers of 4.6 and 0.8, respectively. Therefore, within the primary solvation structure of Zn^{2+}, H_2O makes the main contribution. Following the introduction of NMA, there is an attenuation in the intensity of the Zn^{2+}–H_2O peak, indicative of reduced interaction between water molecules and Zn^{2+} ions. In contrast, the Zn^{2+}–SO_4^{2-} peak experiences an enhancement, suggesting an augmented affinity between sulfate ions and Zn^{2+}. The coordination numbers, which were quantified as 2.6 for Zn^{2+} associated with water molecules and 0.97 for those associated with
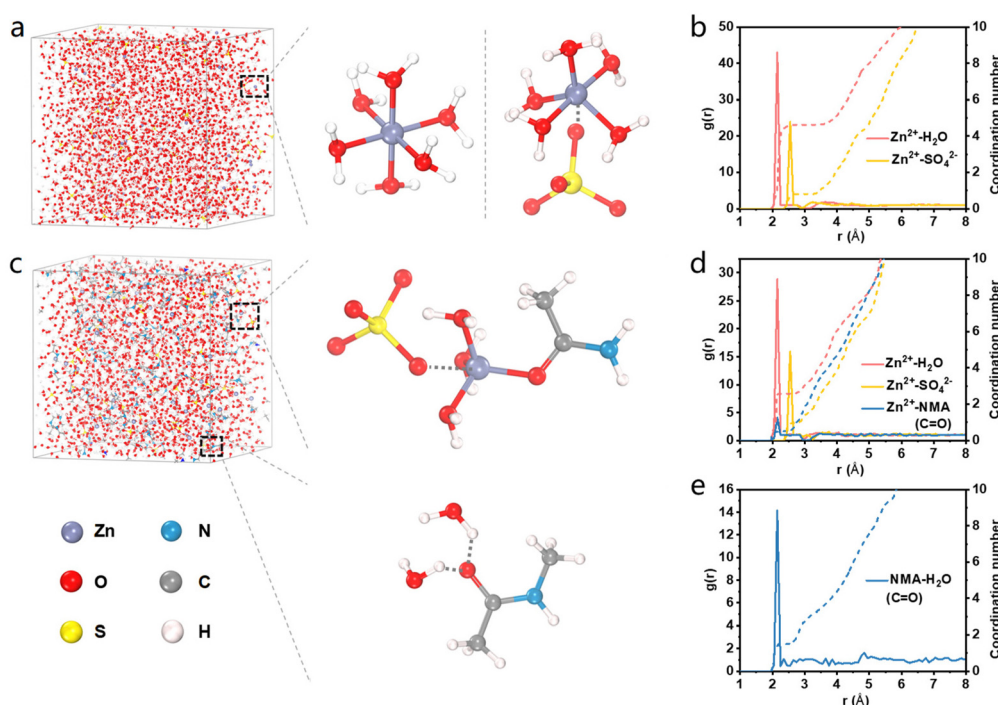
Fig. 2 3D snapshots and corresponding solvation structures of (a) ZS and (c) ZS-25%NMA electrolyte obtained from MD simulations. (b) Radial distribution functions (RDFs) and coordination number of Zn^{2+} in (b) ZS and (d) ZS-25%NMA electrolyte from MD simulations; (e) radial distribution function (RDF) and coordination number of NMA in ZS-25%NMA electrolyte.

sulfate ions, corroborate that NMA facilitates the introduction of SO_4^{2-} into the solvation shell of Zn^{2+} (Fig. 2c and d). Simultaneously, the Zn^{2+}–NMA peak appeared at about 2.15 Å with a coordination number of about 0.5, indicating that a small amount of NMA molecules participate in the main solvation structure of Zn^{2+}. This result is consistent with the conclusions of the Raman spectra and NMR spectra. Furthermore, the radial distribution function and coordination number of the NMA (C=O) molecule were further analyzed. As shown in Fig. 2e, each NMA (C=O) molecule is coordinated with $1.5H_2O$ molecules. This interaction can not only reconstruct the hydrogen bond network of water and directly reduce the activity of water but also reduce the coordination of the water molecules with Zn^{2+} and enhance the interaction between SO_4^{2-} and Zn^{2+}, thereby further reducing the occurrence of the hydrogen evolution reaction.

2.2 Study of the reversibility of zinc anode

Taking into account a multitude of the physicochemical properties of the electrolyte, the formulation containing 25%NMA (denoted as ZS-25%) was selected for further assessment of its electrochemical performance. Under the conditions of 1 mA cm^{-2} and 0.5 mA h cm^{-2}, the initial coulombic efficiency of the Zn//Cu battery using ZS electrolyte is 95.3%, with an internal short circuit occurring after 132 cycles (Fig. 3a). The average coulombic efficiency over all cycles is only 99.33%. Correspondingly, the initial coulombic efficiency of the battery is as high as 97.4% using ZS-25% NMA as the electrolyte, and

stabilizes at around 99.88% after about 200 cycles. The value of batteries using ZS-10% NMA and ZS-35% NMA also reach 99.48% and 99.57% (Fig. S4†). In addition, the battery operates for more than 1200 cycles with an average coulombic efficiency of 99.85%. The significant improvement in coulombic efficiency strongly proves that NMA can anchor water molecules, thus reducing hydrogen evolution and corrosion side reactions at the zinc metal anode. To verify this conclusion, zinc foils were immersed in each of the two electrolytes, and their surface products were then analyzed. As shown in Fig. 3b, the zinc foil shows diffraction peaks of the corrosion product $Zn_4SO_4(OH)_6 \cdot xH_2O$ after immersion in ZS electrolyte for 7 days, and their peak intensity is stronger than that of the zinc foil. Although the diffraction peaks of the corrosion product $Zn_4SO_4(OH)_6 \cdot xH_2O$ also appear on the zinc foil immersed in ZS-25%NMA electrolyte, their intensity is much weaker than that of the former.[1] Therefore, the self-corrosion reaction on the zinc foil surface is greatly suppressed.

2.3 Study of the cycling performance of zinc anode

To further explore the effect of ZS-25%NMA electrolyte on the zinc anode, Zn//Zn symmetric batteries were assembled to evaluate their cycle stability at varying current densities and surface capacities. As shown in Fig. 3c, under the conditions of 1 mA cm^{-2} and 1 mA h cm^{-2}, the symmetric battery using ZS electrolyte experiences an internal short circuit after cycling for only 267 h owing to the severe generation of dendrites on the zinc foil surface. Indeed, the symmetric battery demon-
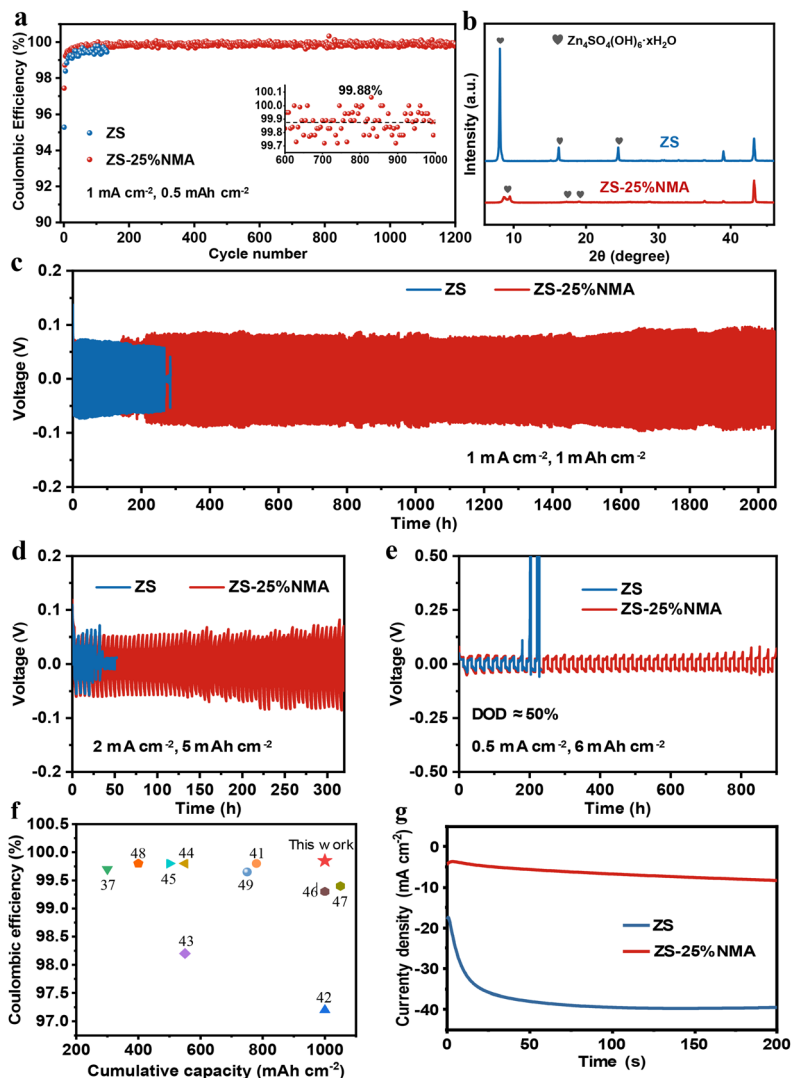
Fig. 3 (a) Coulombic efficiencies of Zn plating/stripping on Cu foil in ZS and ZS-25%NMA electrolytes. (b) XRD patterns of Zn foils after being soaked in ZS and ZS-25%NMA electrolytes for 7 days. Long-term galvanostatic cycling of symmetric Zn cells using ZS and ZS-25%NMA electrolytes at (c) 1 mA cm^{-2} and 1 mA h cm^{-2}, (d) 2 mA cm^{-2} and 5 mA h cm^{-2}, and (e) 0.5 mA cm^{-2} and 6 mA h cm^{-2}, respectively. (f) Comparison of the average CE and cumulative capacity for the ZS-25%NMA electrolyte and other reported electrolytes. (g) Chronoamperometry (CA) tests of Zn//Zn cells with different electrolytes at an overpotential of −150 mV.

strates superior cycle stability, with operational longevity surpassing 2000 h, after the incorporation of 25% NMA into the electrolyte. Correspondingly, the symmetric batteries using ZS-10%NMA and ZS-35%NMA electrolytes also operate normally after 400 h (Fig. S5†). When the current density and surface capacity are further increased to 2 mA cm^{-2} and 5 mA h cm^{-2}, the battery is still able to stably cycle for more than 300 h (Fig. 3d). In contrast, due to the intensified dendrite growth, the zinc foil electrode experiences a short-circuit after cycling in the ZS electrolyte for only 24 h. The service life is significantly reduced to approximately one-thirteenth that achieved in the ZS-25%NMA electrolyte. To further verify the practical potential of ZS-25%NMA electrolyte, the cycling stability of zinc foil electrodes at a high depth of discharge (DOD) were also investigated. Fig. 3e shows the cycling performance

of the Zn//Zn battery assembled with ultrathin (20 μm) zinc foil at 0.5 mA cm^{-2} and 6 mA h cm^{-2} (DOD ≈ 50%). The Zn//Zn battery using ZS-25%NMA electrolyte clearly has a lifespan of more than 900 h, and a stable voltage curve is always maintained. In contrast, the overpotential of the assembled Zn//Zn battery in ZS electrolyte continues to increase during the charge/discharge process and rises sharply at around 175 h, which may be due to serious passivation of the electrode and the production of "dead zinc", resulting in an insufficient amount of available active zinc.[1,29] Fig. 3f shows a comparison of the average coulombic efficiency and cumulative capacity of zinc in ZS-25%NMA electrolyte and in other electrolytes reported in the literature.[37,41–49] The excellent comprehensive performance of the zinc electrode in the ZS-25%NMA electrolyte further demonstrates the effectiveness of the NMA mole-

cules in protecting the zinc anode. The remarkable cycling stability of the zinc electrode is closely related to the uniform nucleation, as shown in Fig. 3g. When an overpotential of −150 mV is applied, the current of the Zn//Zn symmetric battery using the ZS electrolyte exhibits a persistent escalation. This phenomenon is indicative of the prolonged two-dimensional diffusion of Zn^{2+} ions, which leads to a non-uniform nucleation and growth process at the Zn anode surface. In contrast, the exhibited two-dimensional diffusion time is very short for the battery using ZS-25%NMA electrolyte, and then stable diffusion in three-dimensions takes place during the deposition process. This may be related to the adsorption of NMA on the surface of the zinc electrode, which increases the lateral diffusion energy barrier of Zn^{2+}, so that Zn^{2+} creates and maintains more nucleation sites near the initial adsorption point, achieving uniform deposition.[50]

2.4 Morphology and structure analysis of zinc anode after cycling

To verify the positive effect of NMA on zinc deposition, the Zn//Zn symmetric battery was disassembled after 20 cycles to analyze the morphology and structural changes of the zinc anode surface. Under the conditions of 1 mA cm^{-2} and 1 mA h cm^{-2}, the surface of the zinc electrode in the ZS electrolyte is uneven (Fig. S6a†), with a maximum height difference of about 53 μm (Fig. S6b†). Such rugged morphology can easily pierce the separator and cause a short circuit. Additionally, the large exposed surface area will further aggravate corrosion. In contrast, the zinc electrode of the battery using ZS-25%NMA electrolyte shows a smooth and dense morphology (Fig. S6c†) without obvious protrusions or dendrites, and the maximum surface height difference is only about 14 μm (Fig. S6d†).

Furthermore, the zinc electrodes were also characterized after 100 cycles to confirm that the ZS-25%NMA electrolyte can effectively inhibit the interfacial side reactions and dendrite growth. As shown in Fig. 4a, the surface of the zinc foil lost its metallic luster after cycling in the ZS electrolyte, and most of it appears black. This visual alteration is a definitive sign of the irregular deposition/dissolution processes that the zinc underwent, as well as of a severe corrosion reaction. Excitingly, in the ZS-25%NMA electrolyte, the zinc foil still maintains a silvery white shiny surface, demonstrating that the electrolyte
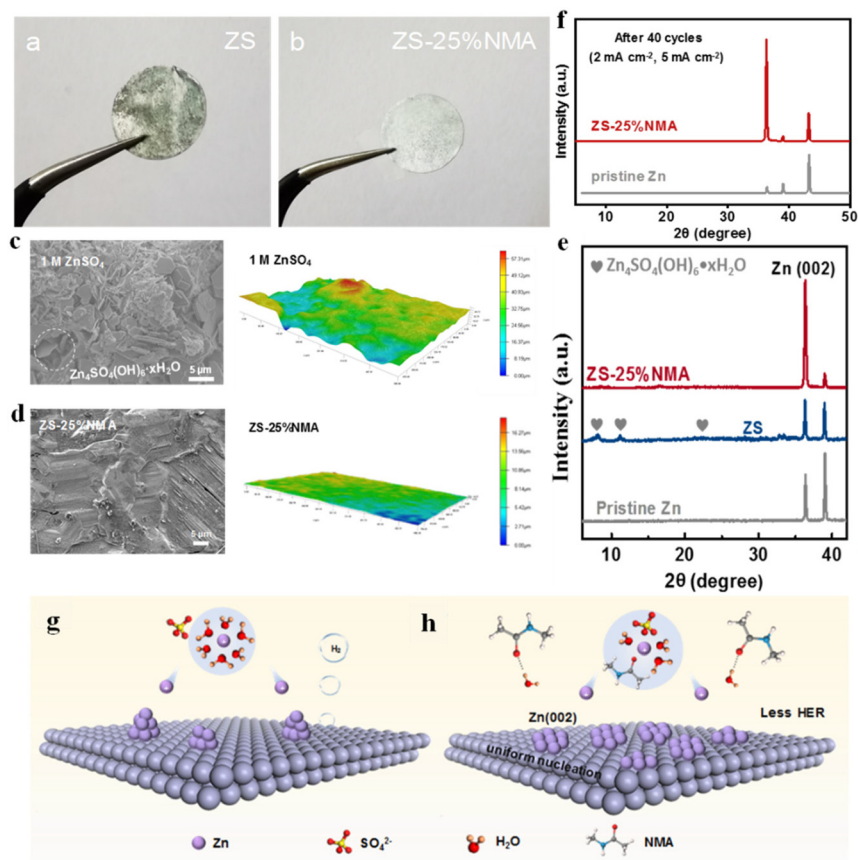

Fig. 4 Digital image of Zn electrode after 100 cycles in (a) ZS electrolyte and (b) ZS-25%NMA electrolyte. SEM and 3D height images of Zn anode after 100 cycles in (c) ZS electrolyte and (d) ZS-25%NMA. (e) XRD patterns of the Zn anodes after 100 cycles. The current density and areal capacity were 1 mA cm^{-2} and 1 mA h cm^{-2}, respectively. (f) XRD patterns of the Zn anodes after 40 cycles at a current density of 2 mA cm^{-2} and areal capacity of 5 mA h cm^{-2}. Schematic illustration of the electrolyte structure and corresponding Zn deposition behavior in (g) ZS and (h) ZS-25%NMA electrolytes.
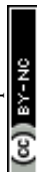
has good compatibility with zinc (Fig. 4b). In addition, it can be seen from the SEM, TEM and optical images (Fig. 4c and Fig. S7b†) that the zinc deposition on the ZS electrolyte shows a loose and porous structure, with an abundance of corrosion byproducts scattered across the surface. This morphology can be used to explain the poor coulombic efficiency and cycle stability of the battery. The uneven zinc deposition can be more clearly observed in the three-dimensional height image (OM); its surface has large undulations, with a maximum height difference of about 57 μm. In contrast, the zinc electrode maintains a flat and dense surface after cycling in the ZS-25%NMA electrolyte (Fig. 4d and Fig. S7a†). The obvious morphological differences further confirm that the NMA molecules have the function of flattening the zinc anode and reducing the hydrogen evolution reaction, thereby improving the lifespan and reversibility of the zinc anode. Additionally, the XRD patterns of the zinc electrodes after 100 cycles (Fig. 4e) show that the peak intensity of the Zn (002) crystal plane is significantly enhanced for the one operated in the ZS-25%NMA electrolyte, while the one used in ordinary electrolyte does not change significantly, indicating that NMA can induce zinc to deposit on the (002) crystal plane. As this crystal plane has a lower surface energy and a higher stacking density, it can further reduce the hydrogen evolution and corrosion reactions of the zinc anode.[51] When the current density and surface capacity are increased, the inductive effect of the ZS-25%NMA electrolyte on the zinc deposition crystal plane becomes more prominent. After 40 cycles at 2 mA cm^{-2} and 5 mA h cm^{-2}, the peak intensity of the Zn (002) crystal plane exceeds that of the Zn (101) crystal plane, and it becomes the dominant crystal plane (Fig. 4f). Together, these results confirm that NMA molecules have the function of regulating the orientation of zinc crystal planes and inducing uniform deposition.

Based on the above results, the protection mechanism of the NMA-based electrolyte on the zinc anode was summarized as shown in Fig. 4g. NMA molecules have high alkalinity and can form strong hydrogen bonds with water, thereby reducing the decomposition activity of water molecules. Simultaneously, NMA promotes the entry of SO$_4^{2-}$ into the Zn^{2+} solvation sheath, and a small number of NMA molecules themselves also participate in the Zn^{2+} solvation sheath, releasing some water molecules around Zn^{2+}, further reducing the hydrogen evolution performance. In addition, the NMA-based electrolyte induces the advantageous exposure of the Zn (002) crystal plane and improves the intrinsic corrosion resistance and uniform deposition ability of the zinc anode, thereby promoting higher reversibility and stability in the deposition/dissolution reactions of the zinc anode.

2.5 Full battery performance study

Subsequently, Zn//NaV$_3$O$_8$ full batteries were assembled and their performances were tested to explore the practical application prospects of ZS-25%NMA electrolyte. The full batteries show a specific capacity of about 140 mA h g^{-1} at 1 A g^{-1} in both ZS and ZS-25%NMA electrolytes (Fig. 5a). However, the battery short circuits at 218 cycles in ZS electrolyte due to
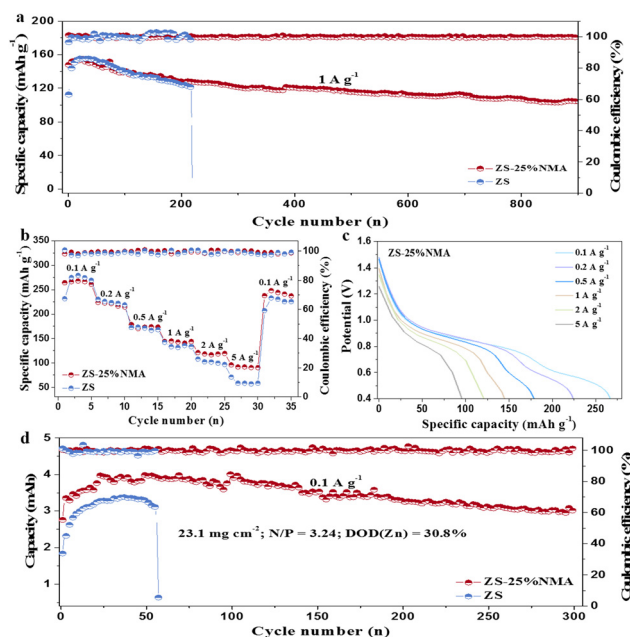

Fig. 5 (a) Cycling performance of Zn//NaV$_3$O$_8$ cells at a current density of 1 A g^{-1}. (b) Rate cycling performance of Zn//NaV$_3$O$_8$ cells with ZS-25%NMA and ZS electrolytes. (c) Galvanostatic discharge profiles of Zn//NaV$_3$O$_8$ cells with ZS-25%NMA electrolyte. (d) Cycling performance of Zn//NaV$_3$O$_8$ cells under high areal capacity.

separator penetration caused by the dendrite growth of the zinc foil anode. Conversely, the battery exhibits enhanced durability when utilized with the ZS-25% NMA electrolyte, achieving over 900 cycles with a commendable capacity retention rate of 70.7%. Moreover, the battery using ZS-25%NMA electrolyte displays better rate cycling performance, especially at high current densities of 2 A g^{-1} and 5 A g^{-1} (Fig. 5b), and higher voltage plateaus (Fig. 5c) than that using the ZS electrolyte (Fig. 5c and S8†) due to the enhanced reversibility of zinc anode with the addition of NMA and lower interface transfer resistance (Fig. S9†).[52] Even under an industrial cathode material load of about 23.1 mg cm^{-2}, the battery using ZS-25% NMA electrolyte shows excellent stability (300 cycles) and capacity retention (82.7%) at 0.1 A g^{-1} with a high discharge depth of the zinc metal anode (DOD ≈ 30.8%, low negative/positive capacity (N/P) ratio of 3.24) (Fig. 5d). The lifespan of the battery using ZS electrolyte pales in comparison; it is only 57 cycles under the same conditions. This series of excellent performances clearly demonstrates the promising practical industrial application prospects of ZS-25%NMA electrolyte.

3. Conclusions

High-basicity NMA has been introduced as a co-solvent to 1 M ZnSO$_4$ electrolyte to alleviate the hydrogen evolution and dendrite growth issues of zinc anodes. Due to its high polarity, NMA can generate strong hydrogen bonds with water molecules, thereby reducing the decomposition activity of water

molecules. Additionally, NMA molecules can promote the entry of SO_4^{2-} into the Zn^{2+} solvation sheath, releasing some water molecules around Zn^{2+}, further reducing the hydrogen evolution performance. NMA molecules promote the uniform nucleation of zinc, laying the foundation for subsequent uniform growth. The NMA-based electrolyte can induce zinc to deposit on the (002) crystal plane, improving the intrinsic corrosion resistance and uniform deposition ability of the zinc anode, thereby promoting the deposition/dissolution of zinc with higher reversibility and achieving a highly stable zinc anode. At a low current density of 1 mA cm^{-2}, the average coulombic efficiency of the zinc electrode after 1200 cycles is as high as 99.85%. The Zn//Zn symmetric battery can operate stably for more than 900 h under high areal capacity and discharge depth conditions (6 mA h cm^{-2}, DOD $\approx$ 50%). Under a low negative capacity/positive capacity (N/P) ratio of 3.24 (high areal capacity of 3.7 mA h cm^{-2}) and a deep discharge depth of the zinc metal anode (DOD $\approx$ 30.8%), the Zn//NaV$_3$O$_8$ full battery achieves a cycle life of 300 cycles with a notable capacity retention rate of 82.7% at a current density of 0.1 A g^{-1}. Undoubtedly, this work will promote the practical application of zinc metal anodes in ZIBs.

Author contributions

Q. Zhang: conceptualization, investigation, writing – original draft preparation, writing – review & editing. H. Fan: methodology, writing – review & editing. J. Gao: funding acquisition. E. Wang: funding acquisition, project administration.

Data availability

The data supporting this article have been included as part of the ESI.†

Conflicts of interest

There are no conflicts to declare.

Acknowledgements

References

1 H. Fan, H. Zhang, Q. Liu, M. Li, L. Liu, J. Gao, Q. Zhang and E. Wang, *ACS Energy Lett.*, 2023, **8**, 4338.

2 J. Chen, Y. Xu, Y. Wang, Z. Lv, S. Zhang, W. Dong, J. Hou, Y. Fang, H. Bi and F. Huang, *Energy Storage Mater.*, 2024, **72**, 103765.

3 H. Yan, S. Li, Y. Nan, S. Yang and B. Li, *Adv. Energy Mater.*, 2021, **11**, 2100186.

4 Y. Li, Z. Wang, Y. Cai, M. E. Pam, Y. Yang, D. Zhang, Y. Wang and S. Huang, *Energy Environm. Mater.*, 2022, **5**, 823.

5 T. Zhou, R. Huang, Q. Lu, P. Liu, L. Hu, K. Zhang, P. Bai, R. Xu, X. Cao, Z. Sun, S. Duan, R. Liu, Y. Qin, X. Sun, Y. Zhang, Y. Li, Y. Yan, M. Liu and X. Wang, *Energy Storage Mater.*, 2024, **72**, 103689.

6 Q. Zhang, H. Fan, Q. Liu, Y. Wu and E. Wang, *J. Mater. Chem. A*, 2024, **12**, 8167.

7 G. Zhang, L. Fu, Y. Chen, K. Fan, C. Zhang, H. Dai, L. Guan, H. Guo, M. Mao and C. Wang, *Angew. Chem., Int. Ed.*, 2024, **63**, e202412173.

8 Z. Jiang, Z. Du, R. Pan, F. Cui, G. Zhang, S. Lei, G. He, K. Yin and L. Sun, *Adv. Energy Mater.*, 2024, **14**, 202402150.

9 W. Du, E. H. Ang, Y. Yang, Y. Zhang, M. Ye and C. C. Li, *Energy Environ. Sci.*, 2020, **13**, 3330.

10 S. Chen, Q. Chen, J. Ma, J. Wang, K. S. Hui and J. Zhang, *Small*, 2022, **18**, 2200168.

11 J. Shi, T. Sun, J. Bao, S. Zheng, H. Du, L. Li, X. Yuan, T. Ma and Z. Tao, *Adv. Funct. Mater.*, 2021, **31**, 2102035.

12 B. Hansen, S. Spittle, B. Chen, D. Poe, Y. Zhang, J. Klein, A. Horton, L. Adhikari, T. Zelovich, B. Doherty, B. Gurkan, E. Maginn, A. Ragauskas, M. Dadmun, T. Zawodzinski, G. Baker, M. Tuckerman, R. Savinell and J. Sangoro, *Chem. Rev.*, 2021, **121**, 1232–1285.

13 Y. Yang, S. Liang, B. Lu and J. Zhou, *Energy Environ. Sci.*, 2022, **15**, 1192–1200.

14 J. Li, S. Qin, M. Xu, W. Wang, J. Zou, Y. Zhang, H. Dou and Z. Chen, *Adv. Funct. Mater.*, 2024, **34**, 2402186.

15 C. W. Li, L. T. Wang, J. C. Zhang, D. J. Zhang, J. M. Du, Y. G. Yao and G. Hong, *Energy Storage Mater.*, 2022, **44**, 104.

16 M. Liu, Q. Zhang, X. Zhang, H. Fan, J. Gao, Z. Jing, M. Wang, Z. Wang and E. Wang, *Chem. Eng. J.*, 2023, **472**, 145154.

17 M. He, J. Chen, A. Hu, Z. Yan, L. Cao and J. Long, *Energy Storage Mater.*, 2023, **62**, 102941.

18 X. Shi, J. Xie, J. Wang, S. Xie, Z. Yang and X. Lu, *Nat. Commun.*, 2024, **15**, 302.

19 R. Qin, Y. Wang, M. Zhang, Y. Wang, S. Ding, A. Song, H. Yi, L. Yang, Y. Song, Y. Cui, J. Liu, Z. Wang, S. Li, Q. Zhao and F. Pan, *Nano Energy*, 2021, **80**, 105478.

20 W. J. Deng, Z. X. Xu and X. L. Wang, *Energy Storage Mater.*, 2022, **52**, 52.

21 L. Yuan, J. Hao, C.-C. Kao, C. Wu, H.-K. Liu, S.-X. Dou and S.-Z. Qiao, *Energy Environ. Sci.*, 2021, **14**, 5669.

22 T. Wang, Z. Tian, Z. You, Z. Li, H. Cheng, W. Li, Y. Yang, Y. Zhou, Q. Zhong and Y. Lai, *Energy Storage Mater.*, 2022, **45**, 24.

23 L. Cao, D. Li, E. Hu, J. Xu, T. Deng, L. Ma, Y. Wang, X.-Q. Yang and C. Wang, *J. Am. Chem. Soc.*, 2020, **142**, 21404.

24 C. P. Li, H. Liu, P. J. Wang, C. B. Deng, B. G. Lu, J. Zhou and S. Q. Liang, *Natl. Sci. Rev.*, 2022, **9**, 1.

25 S. Guo, L. Qin, T. Zhang, M. Zhou, J. Zhou, G. Fang and S. Liang, *Energy Storage Mater.*, 2021, **34**, 545.

26 W. Xu, K. Zhao, W. Huo, Y. Wang, G. Yao, X. Gu, H. Cheng, L. Mai, C. Hu and X. Wang, *Nano Energy*, 2019, **62**, 275.

27 W. Deng, G. Li and X. Wang, *Adv. Funct. Mater.*, 2024, **34**, 2405012.

28 C. Zhu, X. He, Y. Shi, Z. Wang, B. Hao, W. Chen, H. Yang, L. Zhang, H. Ji, J. Liu, C. Yan, J. Zhou and T. Qian, *ACS Nano*, 2023, **17**, 21614.

29 W. Chen, S. Guo, L. Qin, L. Li, X. Cao, J. Zhou, Z. Luo, G. Fang and S. Liang, *Adv. Funct. Mater.*, 2022, **32**, 2112609.

30 J. Zhang, P. Li, Y. Wang, Z. Zhao and Z. Peng, *Adv. Funct. Mater.*, 2023, **33**, 2305804.

31 F. Gao, R. Bai, F. Ferlin, L. Vaccaro, M. Li and Y. Gu, *Green Chem.*, 2020, **22**, 6240.

32 G. Kresse and J. Furthmiiller, *Comput. Mater. Sci.*, 1996, **6**, 15.

33 H. Yang, Z. Chang, Y. Qiao, H. Deng, X. Mu, P. He and H. Zhou, *Angew. Chem., Int. Ed.*, 2020, **59**, 9377.

34 J. Mehringer, E. Hofmann, D. Touraud, S. Koltzenburg, M. Kellermeier and W. Kunz, *Phys. Chem. Chem. Phys.*, 2021, **23**, 1381.

35 Y.-T. Lee, *J. Raman Spectrosc.*, 1997, **28**, 45.

36 P. Xiong, Y. Kang, N. Yao, X. Chen, H. Mao, W.-S. Jang, D. M. Halat, Z.-H. Fu, M.-H. Jung, H. Y. Jeong, Y.-M. Kim, J. A. Reimer, Q. Zhang and H. S. Park, *ACS Energy Lett.*, 2023, **8**, 1613.

37 T. C. Li, Y. Lim, X. L. Li, S. Luo, C. Lin, D. Fang, S. Xia, Y. Wang and H. Y. Yang, *Adv. Energy Mater.*, 2022, **12**, 2103231.

38 J. P. Perdew, K. Burke and M. Ernzerhof, *Phys. Rev. Lett.*, 1996, **77**, 3865.

39 G. Kresse, *Phys. Rev. B:Condens. Matter Mater. Phys.*, 1996, **54**, 11169.

40 P. Zou, R. Lin, T. P. Pollard, L. Yao, E. Hu, R. Zhang, Y. He, C. Wang, W. C. West, L. Ma, O. Borodin, K. Xu, X.-Q. Yang and H. L. Xin, *Nano Lett.*, 2022, **22**, 7535.

41 D. Wang, D. Lv, H. Liu, S. Zhang, C. Wang, C. Wang, J. Yang and Y. Qian, *Angew. Chem., Int. Ed.*, 2022, **61**, e202212839.

42 P. Sun, L. Ma, W. Zhou, M. Qiu, Z. Wang, D. Chao and W. Mai, *Angew. Chem., Int. Ed.*, 2021, **60**, 18247.

43 H. Tian, J. L. Yang, Y. Deng, W. Tang, R. Liu, C. Xu, P. Han and H. J. Fan, *Adv. Energy Mater.*, 2022, **13**, 2202603.

44 H. Wang, W. Ye, B. Yin, K. Wang, M. S. Riaz, B. B. Xie, Y. Zhong and Y. Hu, *Angew. Chem., Int. Ed.*, 2023, **62**, e202218872.

45 K. Zhao, F. Liu, G. Fan, J. Liu, M. Yu, Z. Yan, N. Zhang and F. Cheng, *ACS Appl. Mater. Interfaces*, 2021, **13**, 47650.

46 C. Li, G. Qu, X. Zhang, C. Wang and X. Xu, *Energy Environ. Mater.*, 2023, **7**, e12608.

47 W. Zhang, Y. Dai, R. Chen, Z. Xu, J. Li, W. Zong, H. Li, Z. Li, Z. Zhang, J. Zhu, F. Guo, X. Gao, Z. Du, J. Chen, T. Wang, G. He and I. P. Parkin, *Angew. Chem., Int. Ed.*, 2022, **62**, e202212695.

48 L. Chen, Z. Yang, L. Wang and H. Qin, *Ceram. Int.*, 2019, **45**, 10792.

49 D. Han, T. Sun, H. Du, Q. Wang, S. Zheng, T. Ma and Z. Tao, *Batteries Supercaps*, 2022, **5**, e20220.

50 L. Miao, R. Wang, S. Di, Z. Qian, L. Zhang, W. Xin, M. Liu, Z. Zhu, S. Chu, Y. Du and N. Zhang, *ACS Nano*, 2022, **16**, 9667.

51 T. Wang, J. M. Sun, Y. B. Hua, B. Krishna, Q. Xi, W. Ai and J. S. Yu, *Energy Storage Mater.*, 2022, **53**, 273.

52 Q. Zhang, Q. M. Gao, W. W. Qian, H. Zhang, Y. L. Tan, W. Q. Tian, Z. Y. Li and H. Xiao, *J. Mater. Chem. A*, 2017, **5**, 19136.